ELECTRICAL AND OPTICAL PROPERTIES
OF SEMICONDUCTORS

Resonant Raman Scattering and Dispersion of Polar Optical and Acoustic Phonons in Hexagonal InN

V. Yu. Davydov[a^]**, A. A. Klochikhin**[a, b]**, A. N. Smirnov**[a]**, I. Yu. Strashkova**[a]**, A. S. Krylov**[c]**, Hai Lu**[d]**, William J. Schaff**[d]**, H.-M. Lee**[e]**, Y.-L. Hong**[e]**, and S. Gwo**[e]

[a]*Ioffe Physicotechnical Institute, Russian Academy of Sciences, St. Petersburg, 194021 Russia*
^*e-mail: valery.davydov@mail.ioffe.ru*
[b]*Konstantinov Nuclear Physics Institute, Russian Academy of Sciences, St. Petersburg, 350000 Russia*
[c]*Kirensky Institute of Physics, Russian Academy of Sciences, Krasnoyarsk, 660036 Russia*
[d]*Department of Electrical and Computer Engineering, Cornell University, Ithaca, NY 14853, USA*
[e]*Department of Physics, National Tsing-Hua University, Taiwan, Republic of China*
Submitted August 18, 2009; accepted for publication August 25, 2009

Abstract—It is shown that a study of the dependence of impurity-related resonant first-order Raman scattering on the frequency of excitation light makes it possible to observe the dispersion of polar optical and acoustic branches of vibrational spectrum in hexagonal InN within a wide range of wave vectors. It is established that the wave vectors of excited phonons are uniquely related to the energy of excitation photon. Frequencies of longitudinal optical phonons $E_1(LO)$ and $A_1(LO)$ in hexagonal InN were measured in the range of excitation-photon energies from 2.81 to 1.17 eV and the frequencies of longitudinal acoustic phonons were measured in the range 2.81−1.83 eV of excitation-photon energies. The obtained dependences made it possible to extrapolate the dispersion of phonons $A_1(LO)$ and $E_1(LO)$ to as far as the point Γ in the Brillouin zone and estimate the center-band energies of these phonons (these energies have not been uniquely determined so far).

1. INTRODUCTION

The phonon dispersion curves are considered the important characteristics of vibrational spectrum of a crystal. As a rule, data on these curves are obtained from experiments with scattering of slow neutrons in perfect single-crystal samples with a fairly large size. Such experiments are impossible in the case of InN, which is grown only in the form of epitaxial layers with a thickness no larger than 10 μm. Another method (although less direct, but fairly informative) is Raman spectroscopy; this method makes it possible to obtain information on both phonon energies in the center of the Brillouin zone and these energies at high-symmetry points at the boundary of this zone [1]. However, the data obtained by this method are rather contradictory in the case of hexagonal InN. Even such very important characteristics as the energies of longitudinal optical (LO) phonons at the point Γ of the Brillouin zone have not been established uniquely so far. According to the group-theory analysis, two longitudinal phonons with the symmetry $A_1(LO)$ and $E_1(LO)$ should be observed in the first-order Raman spectrum of hexagonal InN [2]. As was mentioned in previous publications, a feature of the Raman spectrum of hexagonal InN is the presence of lines in the region of 583−591 cm^{-1}; the positions of these lines vary only slightly as the concentration of free electrons is changed within a wide range. These lines were attributed to the $A_1(LO)$ phonons, which have large wave vectors and manifest themselves in the spectrum owing to the Raman process occurring with violation of the law of conservation of the wave vector due to scattering by impurities and defects [3−5]. Agreement between results of theoretical consideration and experimental data was attained [3−5] in the case where the magnitude of the wave vector is larger than the upper boundary of the Landau damping [4] or is much larger than the Thomas—Fermi wave vector [5]. However, the observed spread in the measured frequencies of the $A_1(LO)$ phonon (583−591 cm^{-1}) has not been accounted for so far. An analysis of behavior of phonons with the $E_1(LO)$ symmetry has not been performed in available publications. There are also findings that a change in the energy of excitation photons brings about a variation in a variation in frequencies of both the longitudinal phonon with the symmetry $A_1(LO)$ [6, 7] and the longitudinal phonon with the symmetry $E_1(LO)$ [7] in the Raman spectrum of InN. However, physical factors forming the basis of observed variations have not yet been considered in [6, 7].

In this study, we used the method of Raman spectroscopy to gain insight into dependences of frequencies of vibrations $E_1(LO)$ and $A_1(LO)$ on the energy of excitation photons in hexagonal InN. We show that variations in the frequencies of longitudinal optical

Parameters of InN samples

Sample	InN layer	$n_e,$ cm^{-3}	$n_{Mg},$ cm^{-3}	Thickness, μm
Gs2054	c-InN	3.5×10^{17}	–	5.5
071125	a-InN:Mg	2.8×10^{18}	2×10^{18}	1.3
Gs1810	c-InN:Mg	1.9×10^{18}	6×10^{18}	0.5

vibrations are in the range determined by dispersions of these modes, while the physical mechanism governing the values of wave vectors of these vibrations is the law of conservation of energy in intermediate states of the amplitude of resonance scattering. We also show that, in the presence of impurities, polar acoustic phonons with large wave vectors are active in resonance first-order Raman scattering in InN. Preliminary data obtained in the course of the performed studies were reported in publication [8].

2. EXPERIMENT AND RESULTS

The samples of hexagonal InN were grown by the method of molecular-beam epitaxy with nitrogen plasma activation (MBE NPA). The details of the technological process were reported elsewhere [9, 10]. The main characteristics of the samples are listed in the table. A He−Cd laser, an Ar laser, and a Nd:YAG laser were used to excite the Raman spectra in the range of 2.81−1.17 eV. We used a Jobin−Ivon Horiba T64000 triple Raman spectrometer to measure the Raman spectra as the energy of excitation photons was varied from 2.81 to 1.83 eV. The Raman spectra in the case of excitation with 1.17-eV photons were recorded using a Bruker RFS100/S Raman Fourier spectrometer. All spectra were recorded at room temperature. The backscattering geometry was used in all measurements. A nominally undoped thick c-InN layer (sample Gs2054) grown on the sapphire c plane was used to obtain the data on the frequencies of the E_1(LO) and A_1(LO) phonons in the case of the photon-excitation energy in the range 2.81−1.83 eV. The geometry of scattering from the end face and plane of this layer was used to obtain data on the frequencies of the E_1(LO) and A_1(LO) phonon modes, respectively. The presence of intense luminescence obstructs the measurements of the Raman spectra for undoped InN layers if the photon-excitation energy is 1.17 eV. In order to solve this problem, we studied InN layers doped with Mg. In these layers, luminescence is not observed at room temperature, which made it possible to record with assurance the corresponding Raman spectra. The E_1(LO) mode was studied using the a-InN:Mg sample (sample 071125) grown on the r sapphire plane. The hexagonal axis of the InN layer for this sample features a fixed direction parallel to the substrate surface. The A_1(LO) phonons were studied using a c-InN:Mg sample (Gs1810 sample) grown on the c plane of sapphire.

The hexagonal axis of the InN layer for this sample is directed perpendicularly to the substrate plane.

In Figs. 1a and 1b, we show polarized Raman spectra of undoped c-InN (sample Gs2054); the spectra were measured in the region of optical phonons, normalized to the intensities of the phonon modes A_1(TO) or E_2(high), and shifted along the vertical axis. It can be seen that the frequencies of phonons A_1(TO) (449.0 cm^{-1}) and E_2(high) (491.5 cm^{-1}) do not vary as the energy of excitation photons is varied. However, the phonon lines E_1(LO) and A_1(LO) shift to higher frequencies and increase their intensities as the energy of excitation photons is decreased. For example, in the case of excitation with 2.81-eV photons, the frequencies of these lines are 591.0 cm^{-1} for E_1(LO) and 580.5 cm^{-1} for A_1(LO). When the energy of excitation photons is decreased to 1.83 eV, the corresponding frequencies become equal to 599.0 cm^{-1} for E_1(LO) and 587.5 cm^{-1} for A_1(LO).

In Fig. 2a, we show polarized Raman spectra in the region of optical phonons; the spectra were obtained after an a-InN sample was doped with Mg (the 071125 sample). Measurements with the use of the excitation-photon energies in the range from 2.81 to 1.83 eV showed that light doping with Mg does not affect the frequency of the phonon line E_1(LO) and insignificantly increases the width of this line in comparison with that for an undoped InN sample. These results make it possible to conclude that the Raman spectrum measured for a-InN:Mg can be used to estimate the frequency of the E_1(LO) phonon in the case of excitation with 1.17-eV photons. It was established that E_1(LO) = 602.0 cm^{-1} for this excitation-photon energy.

In Fig. 2b, we show polarized Raman spectra in the range of optical phonons; the spectra were obtained for c-InN:Mg (the sample Gs1810). The Mg concentration in this sample was higher than in the sample of a-InN:Mg (see table). It can be seen that a feature appears on the high-frequency side of the A_1(LO) phonon line in the Raman spectrum of this sample. We relate this feature to manifestation of the E_1(LO) phonon mode prohibited in the scattering geometry under consideration; this mode arises owing to violation of selection rules caused by an increase in the concentration of structural defects as a result of doping with Mg. At the same time, measurements at energies of excitation photons in the range from 2.81 to 1.83 eV showed that the frequency of the A_1(LO) peak was the same for both c-InN:Mg and undoped c-InN. This coincidence of the frequencies makes it possible to use the Raman spectrum of c-InN:Mg to estimate the A_1(LO) phonon frequency in the case of excitation with 1.17-eV photons. It was established that, for this excitation-photon energy, the peak of the A_1(LO) line is at 590.5 cm^{-1}.
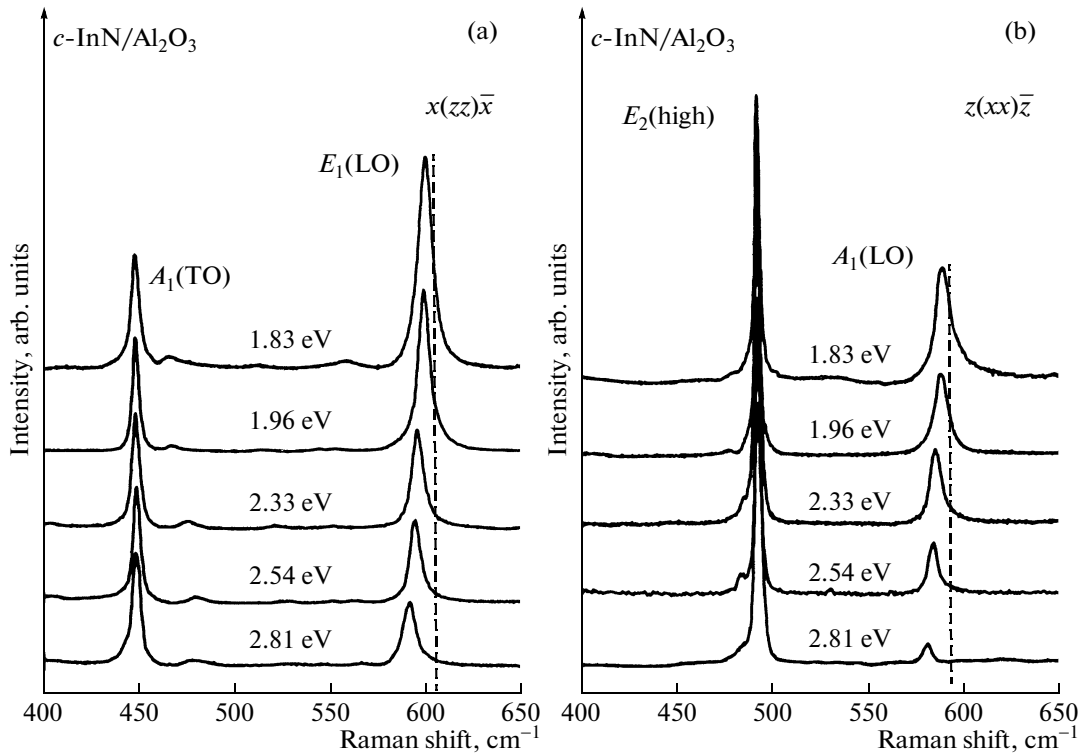
Fig. 1. Polarized Raman spectra of an undoped c-InN (Gs2054) sample; the spectra were obtained at excitation energies in the range from 2.81 to 1.83 eV (indicated at the curves). The scattering geometries $x(zz)\bar{x}$ (Fig. 1a) and $z(xx)\bar{z}$ (Fig. 1b) were used to detect the phonon modes E_1(LO) and A_1(LO), respectively. Here, z is the direction of the InN hexagonal axis. The dashed lines indicate the estimated frequencies of the E_1(LO) and A_1(LO) phonon modes at the point Γ of the Brillouin zone.
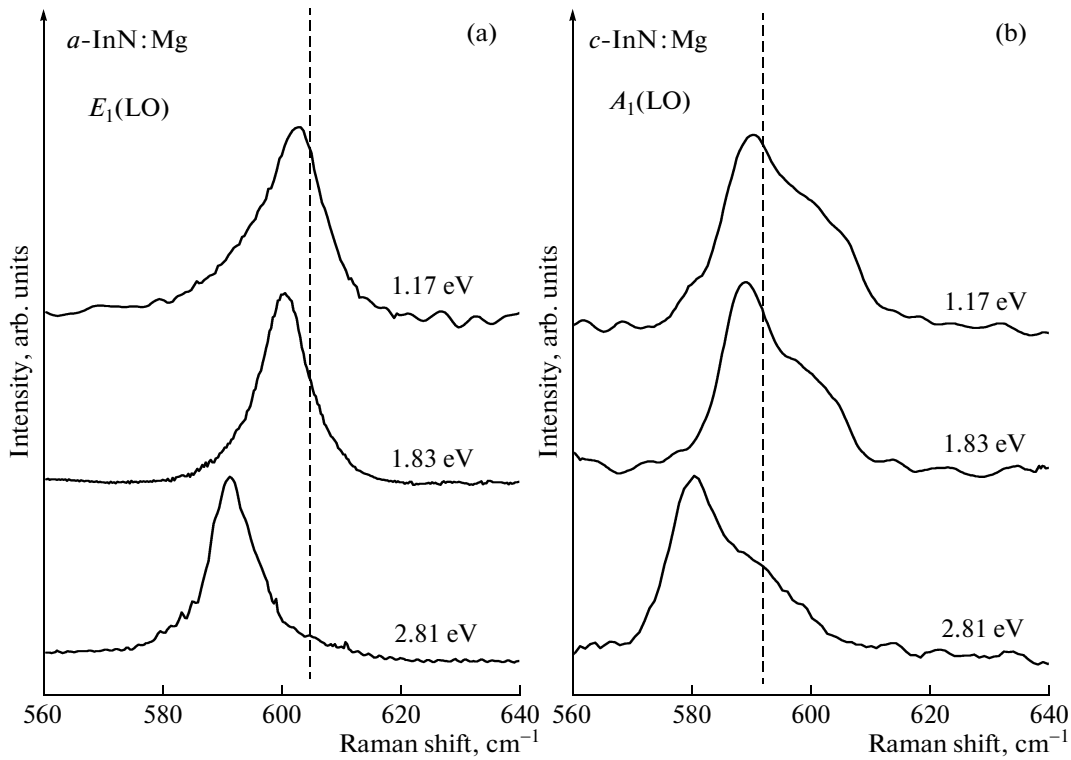
3. THEORY

3.1. Amplitude and Cross Section of Resonant Raman Scattering

Specific features of electronic band structure of InN play an important role in formation of the process of Raman scattering in the region of band-to band absorption. The electronic spectrum of InN in a wide range of energies is characterized by a relative simplicity since the side extrema in the conduction band are absent at the energies as high as about 4 eV [11]. The direct band-to-band electromagnetic transitions from valence bands to the conduction band encompass a wide range of energies and wave vectors of generated electron–hole pairs; the entirety of this range can be considered as the vicinity of a Γ point with the effect of the side extrema disregarded. This makes it possible to describe the resonant Raman process in the effective-mass approximation [12]. As a result of the small value of the band gap ($E_g = 0.67$ eV at low temperatures [13]), this mechanism of Raman scattering in InN is realized in the case of excitation with photons with energies from the infrared to ultraviolet regions of energies. In this case, we observe generation of real electron–hole pairs with an energy equal to the energy of absorbed photons, their subsequent scattering by defects, and final relaxation with excitation of the A_1(LO) and E_1(LO) phonons; this relaxation precedes emission of a scattered photon. The energy and wave vector of relative motion of the electron–hole pair are found to be uniquely related to the energy of excitation or emitted photon. The double resonance in the amplitude of scattering brings it about that the wave vector of a generated phonon (this vector is equal to the wave vector of the center of mass of an electron–hole pair) is found to be related to the wave vector of relative motion; the latter vector is much larger than the wave vector of the incident or scattered photon.

In order to describe the first-order Raman process with the effect of impurity centers taken into account, we have to calculate the amplitude of scattering in the fourth order of the perturbation theory. The expression for the amplitude takes into account the second-order electromagnetic interaction H'_{em}, interaction of photoexcited electron–hole pairs with phonons H_{int}, and interaction of the electron and hole H_i with an impurity center. Schematically, the above expression can be written as

$$A \propto \left\{ \sum_{\lambda, \lambda'} \frac{[H'_{em}]_{0, \lambda}[H_{int}]_{\lambda, \lambda'}[H_i]_{\lambda', \lambda''}[H'_{em}]_{\lambda'', 0}}{\hbar^3(\omega - \Omega_{\lambda, 0})(\omega' - \Omega_{\lambda', 0})(\omega' - \Omega_{\lambda'', 0})} \right\}. \quad (1)$$

Fig. 2. Polarized Raman spectra of the *a*-InN (071125) (a) and *c*-InN (Gs1810) (b) samples doped with Mg; the spectra were obtained at the excitation energies in the range from 2.81 to 1.17 eV (these energies are indicated at the curves). The scattering geometries $x(zz)\bar{x}$ and $z(xx)\bar{z}$ (here, z is the direction of the hexagonal InN axis) were used to detect the phonon modes E_1(LO) and A_1(LO), respectively. The dashed lines indicate the estimated frequencies of the phonon modes E_1(LO) and A_1(LO) at the point Γ.

Here, ω and ω' are the frequencies of the incident and scattered photons and $\Omega_{\lambda, 0}$, $\Omega_{\lambda', 0}$, and $\Omega_{\lambda'', 0}$ are the frequencies of interband transitions.

In what follows, we assume that the electron–phonon interaction of photoexcited electrons and holes is described with the intraband matrix element of the Fröhlich interaction [14], while scattering at a charged center is also described with the intraband matrix element of Coulomb interaction.

In the case of excitation of the Raman process with photons with an energy higher than the absorption threshold, the process becomes resonant in the sense that intermediate states of the scattering amplitude are converted to real ones, rather than being virtual. Looking ahead, we must clarify the limitations imposed on the wave vectors of phonons and related to denominator in the expression (1) for the amplitude if scattering if scattering is excited in the region of intrinsic interband absorption and two denominators in (1) can vanish simultaneously [12]. Properties of the scattering amplitude (1) are similar to those of the amplitude of the second-order Raman scattering, which occurs without involvement of an impurity and results from double intraband interaction with a longitudinal optical phonon [12, 15].

We now write the expression for the amplitude of scattering disregarding the dependence on the wave vectors of the incident and scattered photons and retaining only denominators in the expression for the amplitude; we obtain

$$A(q, \omega) \propto \int \frac{d^3p\, d^3p_1 d^3 p_2}{(\omega - \Omega_p^{\text{eh}})(\omega' - \Omega_{p_2}^{\text{eh}})(\omega_1 - \Omega_{p_1}^{\text{eh}} - \hbar q^2/2M)}$$
$$\times [\delta(\mathbf{p} - \mathbf{p}_1 + \mathbf{q}^e) - \delta(\mathbf{p} - \mathbf{p}_1 + \mathbf{q}^h)] \tag{2}$$
$$\times [\delta(\mathbf{p}_1 - \mathbf{p}_2 + \mathbf{q}^e) - \delta(\mathbf{p}_1 - \mathbf{p}_2 + \mathbf{q}^h)],$$

where $\Omega_p^{\text{eh}} = E_g/\hbar + \hbar p^2/2\mu$, E_g is the band gap, $\mu = m_e m_h/(m_e + m_h)$ is the reduced effective mass of an electron and a hole, M is the translational mass of the pair, $q^{e, h} = q\mu/m_{e, h}$, and $\hbar^2 p^2/2\mu$ is the kinetic energy of relative motion of an electron–hole pair.

The complete expression for the amplitude of scattering includes two terms of type (2). In the first term, the amplitudes $\omega_1 = \omega$. In the second term, the amplitudes are obtained as a result of substitution $\omega_1 = \omega'$, where ω and ω' are the frequencies of the incident and scattered photons.

Integration with respect to d^3p_1 and d^3p_2 is performed using the δ functions. As a result, we obtain

$$A(q, \omega) \propto \frac{v_c}{(2\pi)^3} \int d^3p \left[\frac{1}{D(\omega, p)D^e(\omega', \mathbf{p} - \mathbf{q})D(\omega', p)} \right.$$
$$\left. - \frac{1}{D(\omega, p)D^h(\omega', \mathbf{p} - \mathbf{q})D^\mu(\omega, \mathbf{p} - \mathbf{q})} \right], \quad (3)$$

where v_c is the volume of an elementary cell and

$$D(\omega, p) = \left(\Delta - \frac{\hbar p^2}{2\mu} + i\gamma \right),$$

$$D^e(\omega', \mathbf{p} - \mathbf{q}) = \Delta' - \frac{\hbar(\mathbf{p} - \mathbf{q})^2}{2m_e} - \frac{\hbar p^2}{2m_h} + i\gamma,$$

$$D^h(\omega', \mathbf{p} - \mathbf{q}) = \Delta' - \frac{\hbar(\mathbf{p} - \mathbf{q})^2}{2m_h} - \frac{\hbar p^2}{2m_e} + i\gamma,$$

$$D(\omega', p) = \Delta' - \frac{\hbar p^2}{2\mu} + i\gamma,$$

$$D^\mu(\omega', \mathbf{p} - \mathbf{q}) = \Delta' - \frac{\hbar(\mathbf{p} - \mathbf{q})^2}{2\mu} + i\gamma.$$

Here, $\Delta = (\omega - E_g/\hbar)$, $\Delta' = (\omega' - E_g/\hbar)$, and γ is the decay of electron–hole pairs in intermediate states. Yet another contribution to the amplitude is obtained by the replacement $m_e \rightleftharpoons m_h$, and, finally, an additional two terms are obtained from derived expressions using the substitution $\Delta \rightleftharpoons \Delta'$.

Integration with respect to the angle between the vectors $\mathbf{p}$ and $\mathbf{q}$ yields the following expression after summation of all terms:

$$A(q, \omega) \propto \frac{v_c}{(2\pi)^2} \int p^2 dp \frac{(m_e + m_h)}{\hbar p q} \frac{1}{D(\omega, p)D(\omega', p)}$$
$$\times \{ [-L_\mu(\Delta) + L_{m_e}(\Delta) + L_{m_h}(\Delta)] \quad (4)$$
$$+ [-L_\mu(\Delta') + L_{m_e}(\Delta') + L_{m_h}(\Delta')] \},$$

where

$$L_\mu(\Delta) = \ln \left[\frac{\Delta - \dfrac{\hbar(p - q)^2}{2\mu} + i\gamma}{\Delta - \dfrac{\hbar(p + q)^2}{2\mu} + i\gamma} \right], \quad (5)$$

$$L_{m_e}(\Delta) = \ln \left[\frac{\Delta - \dfrac{\hbar(p - q)^2}{2m_e} - \dfrac{\hbar p^2}{2m_h} + i\gamma}{\Delta - \dfrac{\hbar(p + q)^2}{2m_e} - \dfrac{\hbar p^2}{2m_h} + i\gamma} \right], \quad (6)$$

while the expression for $L_{m_h}(\Delta)$ is obtained from (6) by ireplacement $m_e \longrightarrow m_h$.

The remaining three functions are obtained by the replacement $\Delta \longrightarrow \Delta'$.

3.2. Interference of Resonant Terms in the Amplitude of Scattering and Separation of Wave Vectors of Phonons

In what follows, we show that the interference of contributions (caused by real processes of absorption of incident photons and emission of scattered photons) to the amplitude of scattering brings about a limitation imposed on the magnitude of phonons' wave vectors. For the sake of simplicity, we will disregard the decay of electron–hole pairs in intermediate states in this consideration and represent the real and imaginary parts of the first and second denominators in (4) as

$$D(\omega, p) = \frac{1}{(\Delta - \hbar p^2/2\mu)p} + i\pi\delta\left(\Delta - \frac{\hbar p^2}{2\mu}\right) \quad (7)$$

and

$$D(\omega', p) = \frac{1}{(\Delta' - \hbar p^2/2\mu)p} + i\pi\delta\left(\Delta' - \frac{\hbar p^2}{2\mu}\right). \quad (8)$$

We then integrate expression (4) with respect to dp^2 using δ functions from (7) and (8); these functions express the law of conservation of energy in the course of electromagnetic transitions.

We now consider in more detail the contributions to the scattering amplitude as induced by the terms $L_\mu(\Delta)$ and $L_\mu(\Delta')$:

$$A(q, \omega) \propto \left[\frac{2\mu(m_e + m_h)v_c}{(2\pi)^2 \hbar^2 q} \right] \frac{2\mu}{\hbar(p_\omega + p_{\omega'})} \frac{1}{(p_\omega - p_{\omega'})}$$
$$\times \{ [\ln(2p_\omega - q) - \ln(2p_{\omega'} - q)]$$
$$- [\ln(2p_\omega + q) - \ln(2p_{\omega'} + q)] \}.$$

Here, $p_\omega = \sqrt{2\mu\Delta/\hbar}$ and $p_{\omega'} = \sqrt{2\mu\Delta'/\hbar}$. Taking into account that

$$p_\omega, p_{\omega'} \gg (p_\omega - p_{\omega'})$$

we can replace the ratio of differences with the derivative

$$\frac{1}{(p_\omega - p_{\omega'})} [\ln(2p_\omega - q) - \ln(2p_{\omega'} - q)]$$

$$\approx \frac{d}{dp_\omega} \ln(2p_\omega - q) = \frac{1}{(2p_{\omega'} - q)}.$$

All remaining contributions to the scattering amplitude are also transformed similarly; as a result, this amplitude is found to be proportional to $1/(2p_\omega - q)$ or $1/(2p_{\omega'} - q)$.

The cross section of scattering is bound to involve the squared moduli of the above expressions. Thus, the wave vector of a phonon is found to be equal to $q = 2p_\omega$ or $q = 2p_{\omega'}$; i.e., this wave vector is determined by the wave vector of relative motion of an electron–hole pair. The latter wave vector, in turn, is determined by the frequency of excitation or scattered photon.

3.3. Cross Section of Scattering

We now study the cross section of scattering with the decay of an electron–hole pair in the intermediate

state γ taken into account. To this end, we represent one of the terms, for example, $L_{m_e}(\Delta)$, at $p = p_\omega$ as

$$L_{m_e}(\Delta) = \ln\left[\frac{2p_\omega - q + i2m_c\gamma/\hbar q}{-2p_\omega - q + i2m_c\gamma/\hbar q}\right].$$

Thus, in order to take into account the decay, it is sufficient to perform the following replacement:

$$\frac{1}{(2p_\omega - q)} \longrightarrow \frac{1}{(2p_\omega - q) + i2m\gamma/\hbar q};$$

here, $m = m_e$, m_h, or μ.

As a result, the contribution (due to interference of real electromagnetic transitions) to the amplitude of scattering can be represented as

$$A(q, \omega) \propto \left[\frac{2\mu(m_e + m_h)v_c}{(2\pi)^2\hbar^2 q}\right]\frac{2\mu}{\hbar(p_\omega + p_{\omega'})}$$

$$\times \left[\frac{p_\omega}{(p_\omega^2 - q^2/4 - i\mu\gamma/\hbar)} + \frac{p_{\omega'}}{(p_{\omega'}^2 - q^2/4 - i\mu\gamma/\hbar)}\right].$$ (9)

When calculating the cross section of scattering, it is also necessary to take into account the screening of the Coulomb interaction of electrons and holes with impurity centers by free charge carriers:

$$H_i(q) = \frac{4\pi Ze}{v_c q^2[\varepsilon_\infty + \chi_\mathbf{q}(0)]} \approx \frac{4\pi Ze}{v_c\varepsilon_\infty[q^2 + q_{TF}^2]};$$ (10)

here, $\chi_\mathbf{q}(0)$ is the susceptibility of free electrons in the static limit, $q_{TF} = \sqrt{3\omega_{pl}^2/v_F^2}$ is the Thomas−Fermi wave vector, ω_{pl} is the frequency of plasma oscillations at the zero wave vector, and v_F is the velocity of electrons at the Fermi surface.

The final expression for the cross section of scattering due to the Fröhlich interaction and scattering of an electron−hole pair at charged impurities is obtained as a result of integration of the squared modulus of the scattering amplitude with respect to dq^2:

$$\sigma(\omega) \propto \frac{N_i}{2\pi^2} \frac{p_\omega}{(p_\omega + p_{\omega'})^2}\left|\frac{4\pi Ze}{v_c\varepsilon_\infty(4p_\omega^2 + q_{TF}^2)}\right|^2 \frac{1}{\mu\gamma/\hbar}$$

$$\times \frac{2\pi}{\hbar}\delta[\omega - \omega' - \Omega_{LO}(q = 2p_\omega)];$$ (11)

here, N_i is the concentration of impurity centers. A similar contribution arises owing to a resonance with scattered light and is obtained from (11) if the replacement $p_\omega \rightleftharpoons p_{\omega'}$ is used.

As long as the value of q is beyond the limits of the upper boundary for the Landau decay, i.e., as long as

$$2p_\omega > 2p_F + \sqrt{2m^*\Omega_{LO}/\hbar},$$

a nonscreened phonon of longitudinal optical branch appears at $q \approx 2p_\omega$ as a result of the event of resonance scattering. This form of the cross section is characteristic of InN samples with a not very high electron concentration. As follows from expression (9), the magnitudes of the wave vectors of phonons are determined to

the accuracy of decay of an electron−hole pair, i.e., $q = 2p_\omega \pm \sqrt{2\mu\gamma/\hbar}$ and $q = 2p_{\omega'} \pm \sqrt{2\mu\gamma/\hbar}$. Thus, the range of magnitudes of phonons' wave vectors increases as the decay of electron−hole pairs becomes more significant.

4. DISCUSSION OF THEORETICAL RESULTS AND EXPERIMENTAL DATA

4.1. Dispersion of Electron Bands and Longitudinal Optical Branches

The above analysis of the amplitude of a resonant Raman process in relation to the Fröhlich interaction of LO vibrations with electrons and holes and to intraband scattering of electron−hole pairs by charged impurities showed that the wave vector of a phonon q is determined by the frequency of excitation of scattered light. At the same time, it follows from expression (4) that the magnitude of phonon's wave vector depends on dispersion of energy of an electron−hole pair. Available data on photoemission in InN [16, 17] make it possible to determine both the dispersion of the conduction band and dispersions of the bands of light and heavy holes. In Fig. 3a, we plotted the results of our calculations of dispersions of these bands and the dispersion of electron−hole pairs arising as a result of vertical transitions from the bands of heavy and light holes to the conduction band. As was shown by Klochikhin et al. [18], the dispersion of electron band in InN is adequately described by the following expression (with nonparabolicity taken into account):

$$\varepsilon^e(k) = E_e\left\{\sqrt{\hbar^2 k^2/2m_\Gamma^e E_e + 1/4} - 1/2\right\}.$$ (12)

Here, m_Γ^e is the effective mass of an electron at the point Γ ($m_\Gamma^e = 0.07m_0$) and E_e is the parameter of nonparabolicity ($E_e = 0.4$ eV). A similar expression was used for nonparabolic dispersion of the band of light holes; i.e.,

$$\varepsilon^{lh}(k) = -E_{lh}\left\{\sqrt{\hbar^2 k^2/2m_\Gamma^{lh} E_{lh} + 1/4} - 1/2\right\},$$ (13)

where m_Γ^{lh} is the effective mass of a light hole at the point Γ ($m_\Gamma^{lh} = 0.035m_0$) and E_{lh} is the parameter of nonparabolicity ($E_{lh} = 0.8$ eV). A parabolic approximation with $m^{hh} = 0.4m_0$ was used for the band of heavy holes. The dispersion of an electron−hole pair is obtained as the difference between dispersion curves for the conduction band and the corresponding curve for one of the valence bands. In plotting the dispersion curves shown in Fig. 3a, we used the value of the InN band gap at room temperature ($E_g = 0.63$ eV [13]).

The magnitudes of the wave vectors of the phonons generated as a result of scattering correspond to the doubled magnitude of the wave vector at which the horizontal straight line drawn at the level of the excitation-photon energy intersects the dispersion curves for electron−hole pairs. As can be seen from Fig. 3, these magnitudes differ markedly for the pairs consisting of light and heavy holes and an electron.

That the position of the A_1(LO) line in the Raman spectra monotonically shifts to lower frequencies as the energy of the excitation photon is varied from 1.17 to 2.81 eV (Fig. 1b) is of extreme importance for the subsequent analysis. This variation in the energy corresponds to the change in the phonon's wave vector from 0.115×10^8 to 0.335×10^8 cm^{-1} if the transition from the band of light holes is realized in the course of scattering and from 0.28×10^8 to 0.68×10^8 cm^{-1} for transitions with involvement of heavy holes.

The branch A_1(LO) exists only in the direction $\Gamma−A$ of the Brillouin zone in hexagonal InN, and its frequency decreases from a maximum value at the point Γ to a minimum value at the zone boundary [19]. The limiting magnitude of the wave vector at the boundary of the Brillouin zone is equal to 0.55×10^8 cm^{-1}. A monotonic decrease in the frequency as the wave vector is increased is possible if the magnitude of the wave vector is no larger than the boundary value. This condition is fulfilled for transitions from the band of light holes and is not fulfilled for transitions from the band of heavy holes. Thus, only the electron−hole pairs arising as a result of transition from the band of light holes to the conduction band are involved in formation of the Raman process with excitation of an A_1(LO) phonon.

The situation is more complex for the E_1(LO) branch, which exists in a larger portion of the space of the Brillouin zone. In this case, both electromagnetic transitions from the band of light holes and transitions from the band of heavy holes can be involved in formation of the Raman process with excitation of an E_1(LO) phonon.

In Fig 3b, we show the dispersion of LO branches as a function of the wave vectors corresponding both to transitions from the band of light holes and to transitions from the band of heavy holes. For the studied InN samples and the used energies of excitation photons, the minimum magnitudes of the wave vectors are found to be beyond the upper boundary of the Landau decay q_L^+; this boundary (with nonparabolicity of the conduction band taken into account) amounts to $q_L^+ = 0.08 \times 10^8$ and 0.111×10^8 cm^{-1} for concentrations 3.5×10^{17} and 2.0×10^{18} cm^{-3}, respectively. Thus, only unbound LO phonons exist beyond this boundary. Extrapolation of dispersions of the LO modes makes it possible to estimate their frequencies at the Γ point of the Brillouin zone; these frequencies were found to be
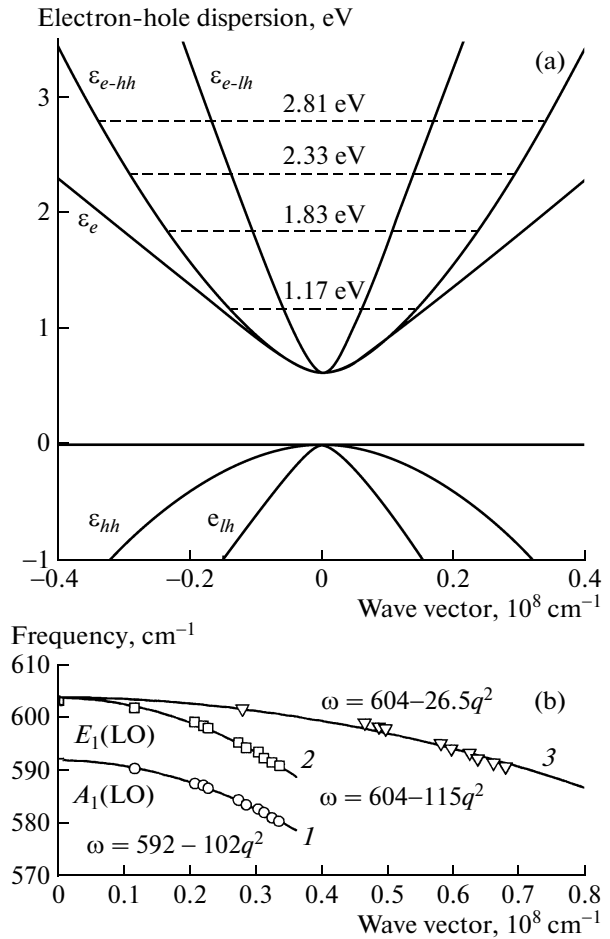
Fig. 3. (a) Dispersion of the valence bands, conduction band, and electron−hole pairs in InN. Horizontal lines correspond to the energies of excitation photons. (b) Frequencies of the A_1(LO) and E_1(LO) phonons in relation to the wave vector of a phonon $q = 2p_\omega$. The wave vectors are calculated for transitions from the band of light holes (curves 1, 2) and transitions from the band of heavy holes (curve 3). Triangles, squares, and circles represent experimental data. Solid lines represent an approximation of dispersion of the A_1(LO) and E_1(LO) branches with a square-law function.

equal to A_1(LO) = 592 and E_1(LO) = 604 cm^{-1}. It can be seen that, for both transitions from the band of light holes and transitions from the band of heavy holes, the frequency of the E_1(LO) phonon at the Γ point is found to be identical.

In Fig. 4, we show calculated dispersion phonon curves for hexagonal InN; the data were taken from [19]. Experimental data for the A_1(LO) branch along the $\Gamma−A$ direction are also shown in Fig. 4. The wave vectors in this case were calculated on the assumption of electromagnetic transitions from the band of light holes. The wave vectors for the E_1(LO) branch along the $\Gamma−K$ direction are obtained assuming that there are electromagnetic transitions from the band of light

Fig. 4. The phonon dispersion curves for hexagonal InN (taken from [19]) and experimental data obtained in this study (circles and triangles).

Fig. 5. Polarized Raman spectra of (*1*) undoped InN samples and InN samples doped with Mg with N_{Mg} = (*2*) 6.0×10^{18}, (*3*) 4.6×10^{19}, (*4*) 7.3×10^{19}, (*5*) 2.4×10^{20}, (*6*) 7.1×10^{20}, (*7*) 1.4×10^{21}, and (*8*) 5.5×10^{21} cm^{-3}. The scattering geometry was $z(xx)\bar{z}$, where z is the direction of the InN hexagonal axis.

holes, while the corresponding vectors along the $\Gamma-M$ direction are obtained for transitions from the band of heavy holes. It can be seen that the experimental data and the results of modeling calculations of dispersion curves for LO phonons are in satisfactory agreement.

As it was mentioned above, the Raman studies of hexagonal InN involve many inconsistencies in the measured frequencies of the A_1(LO) phonons in the range 586–591 cm^{-1}. In addition, the excitation-photon energies used in all measurements were, as a rule, close to each other (2.54 or 2.41 eV). In order to clarify the cause of so large discrepancies, we studied the InN samples with controlled number of structural defects generated as a result of doping with Mg. The samples were grown by the MBE NPA method on the c plane of sapphire and the Si (111) substrates [9, 11]. All samples featured the wurtzite structure with the hexagonal axis directed perpendicularly to substrates' planes. According to the data of secondary-ion mass spectrometry. the Mg concentration varied from $N_{Mg} = 6.0 \times 10^{18}$ to 5.5×10^{21} cm^{-3}.

In Fig. 5, we show the Raman spectrum of undoped InN sample and the spectra of the c-InN:Mg samples with the Mg concentration varying within a wide range. It can be seen that, at a relatively low level of doping, a wing appears at the high-frequency edge of the A_1(LO) line; this wing shifts to higher frequencies as the Mg concentration is increased and becomes a prevailing feature of the spectrum. We observed such transformation of the spectrum at all excitation energies within the range from 2.81 to 1.83 eV.

We also relate the observed changes in the Raman spectrum to the resonance features of the process of Raman scattering in c-InN:Mg. The above analysis of

the amplitude of the resonance Raman process showed that magnitudes of the phonon wave vectors are determined to the accuracy of decay of an electron–hole pair. The A_1(LO) branch is strictly defined only along the hexagonal axis. As the concentration of defects caused by doping with Mg increases (and, as a result, the decay of electron–hole pairs increases), the range of the wave vectors of phonons involved in the process of scattering widens. In addition, the region of the E_1(LO) branch where the density of states is much higher becomes involved. This makes it possible to gain insight into the transformation of the Raman spectra as the Mg concentration is increased by relating this transformation to manifestation of the E_1(LO) phonon mode; the latter is prohibited in the scattering geometry under consideration.

These results make also possible to understand the cause of discrepancies in measured frequencies of an A_1(LO) phonon in nominally undoped InN samples. It can be assumed with a high degree of confidence that, at the identical excitation energy, the measured frequency of the line in the scattering geometry making it possible to observe A_1(LO) phonons should be higher if the studied InN sample contains a larger number of structural defects.

Fig. 6. Polarized Raman spectra of an undoped c-InN (Gs2054) sample in the region of acoustic vibrations; the spectra were obtained for various excitation energies (indicated at the curves) and the scattering geometry (a) $x(zz)\bar{x}$ and (b) $z(xx)\bar{z}$ (here, z coincides with the direction of the hexagonal axis). The spectra are normalized to the intensity of the corresponding Raman lines.

4.2. Dispersion of Longitudinal Acoustic Branches in InN

The selection of phonons' wave vectors in the cross section of scattering (11) arises as a result of double resonance in the amplitude of scattering in the case of excitation in the region of band-to-band transitions. The important condition consists in the requirement for intraband character of both the Fröhlich interaction of electrons and holes with longitudinal optical phonons and scattering at charged impurities. All these conditions are also satisfied in the case of scattering with excitation of polar acoustic phonons, the intraband interaction of which with photoexcited electron–hole pairs is very similar to the Fröhlich interaction of polar optical phonons. An experimental study of scattering in the region of acoustic branches of the vibrational spectrum showed that the lines corresponding to the energies of acoustic phonons at large wave vectors appear in the InN Raman spectra.

In Fig. 6a, we show the polarized Raman spectra of undoped c-InN (sample Gs2054) in the region of acoustic phonons; the spectra were obtained in the $x(zz)\bar{x}$ scattering geometry using the excitation energies in the range from 2.71 to 1.83 eV. It can be seen that, as the excitation energy is decreased, the line monotonically shifts to lower frequencies. This shift amounts to 45 cm^{-1} within the range of used excitation energies. The wave vectors of phonons vary in the range $(0.46-0.66) \times 10^8$ cm^{-1} if it is assumed that scattering occurs with involvement of electromagnetic transitions from the band of heavy holes. The dependence of the phonon frequency on the wave vector is almost linear. This makes it possible to determine the sound velocity; as a result of linear extrapolation of experimental data, this velocity is found to be equal to 5220 m/s.

In Fig. 6b, we show the polarized Raman spectra (of the same sample) observed in the region of acoustic branches in the $z(xx)\bar{z}$ scattering geometry and in the same range of excitation. In this case, the phonon line shifts by 57 cm^{-1}. The dependence of phonon frequency on the wave vector is also practically linear if it is assumed that scattering occurs with involvement of electromagnetic transitions from the band of heavy holes; the sound velocity obtained by linear extrapolation is found to be equal to 5430 m/s.

It is of interest to compare the obtained dispersions of acoustic phonons with the results of calculations of dynamics of the InN crystal lattice [19]. This comparison is presented in Fig. 4 where the data obtained in the $x(zz)\bar{x}$ and $z(xx)\bar{z}$ scattering geometries are plotted in the $\Gamma-M$ and $\Gamma-K$ directions, respectively. The sound velocities obtained from experimental data are found to be close to the calculated values extrapolated

from the region of small wave vectors (5170 and 5050 m/s in the $\Gamma-M$ and $\Gamma-K$ directions, respectively). This indicates that our choice of wave vectors due to electromagnetic transitions from the band of heavy holes is justified. In addition, experimental data demonstrate the dependence of frequency on the wave vector; this dependence is almost linear in a wider range of wave vectors than calculated curves.

It is worth noting that longitudinal acoustic (LA) phonons are observed (in contrast to optical phonons) in the $z(xx)\bar{z}$ scattering geometry; these LA phonons have wave vectors that can be caused only by electromagnetic transitions from the band of heavy holes since it is only in this case that the velocity of sound has a realistic value. This may be indicative of a difference between the selection rules for optical and acoustic phonons.

The absence of acoustic phonons in the region below 80 cm^{-1} in the spectrum measured in this geometry (such phonons may be related to the $\Gamma-A$ direction and wave vectors corresponding to transitions from the band of light holes) can be associated with a lower density of vibrational states in this direction.

In order to obtain a more detailed pattern of the behavior of acoustic phonons, we should perform new calculations of the InN vibrational spectrum and selection rules for acoustic branches at large wave vectors; additional experimental studies of scattering in this region are also needed.

5. CONCLUSIONS

We demonstrated new possibilities of the first-order impurity resonance Raman scattering, which make it possible to reconstruct the dispersion of polar optical and acoustic phonons in a wide range of wave vectors by studying the cross section of scattering as a function of the energy of excitation photons. We showed that the wave vectors of phonons are found to be uniquely related to the energy of excitation photon. As a result, the dispersion of longitudinal optical phonons and longitudinal acoustic phonons in InN is recovered in a wide range of wave vectors. The frequencies of the longitudinal optical branches obtained by extrapolation to the point Γ were found to be equal to $A_1(LO) = 592$ and $E_1(LO) = 604$ cm^{-1}. The obtained results may be useful for future calculations of dynamics of the crystal lattice of hexagonal InN.

ACKNOWLEDGMENTS

REFERENCES

1. M. Cardona, *Light Scattering in Solids II*, ed. by M. Cardona and G. Güntherodt (Springer, 1982) p. 19.
2. C. A. Arguello, D. L. Rousseau, and S. P. S. Porto, Phys. Rev. **181**, 1351 (1969).
3. A. Kasic, M. Schubert, Y. Saito, Y. Nanishi, and G. Wagner, Phys. Rev. B **65**, 115206 (2002).
4. J. S. Thakur, D. Haddad, V. M. Naik, R. Naik, G. W. Auner, H. Lu, and W. J. Schaff, Phys. Rev. B **71**, 115203 (2005).
5. F. Demangeot, C. Pinquier, J. Frandon, M. Gaio, O. Briot, B. Maleyre, S. Ruffenach, and B. Gil, Phys. Rev. B **71**, 104305 (2005).
6. R. Cuscó, J. Ibáñez, E. Alarcón-Lladó, L. Artús, T. Yamaguchi, and Y. Nanishi, Phys. Rev. B **79**, 155210 (2009).
7. V. Yu. Davydov and A. A. Klochikhin, *Indium Nitride and Related Alloys*, Ed. by T. D. Veal, C. F. McConville, and W. J. Schaff (CRC Press, Boca Raton, 2009) p. 208.
8. V. Yu. Davydov, A. A. Klochikhin, A. N. Smirnov, I. Yu. Strashkova, A. S. Krylov, Hai Lu, W. J. Schaff, H.-M. Lee, Y.-L. Hong, and S. Gwo, Phys. Rev. B **80**, 081204(R) (2009).
9. H. Lu, W. J. Schaff, J. Hwang, H. Wu. W. Yeo, A. Pharkya, and L. F. Eastman, Appl. Phys. Lett. **77**, 2548 (2000).
10. Y.-M. Chang, Y.-L. Hong, and S. Gwo, Appl. Phys. Lett. **93**, 131106 (2008).
11. F. Bechstedt and J. Furthmüller, J. Cryst. Growth **246**, 315 (2002).
12. R. M. Martin, Phys. Rev. B **10**, 2620 (1974).
13. A. A. Klochikhin, V. Yu. Davydov, V. V. Emtsev, A. V. Sakharov, V. A. Kapitonov, B. A. Andreev, H. Lu, and W. J. Schaff, Phys. Rev. B **71**, 195207 (2005).
14. J. Menendez and M. Cardona, Phys. Rev. B **31**, 3696 (1985).
15. A. A. Abdumalikov and A. A. Klochikhin, Phys. Stat. Solidi B **80**, 43 (1977).
16. L. Colakerol, T. D. Veal, H.-K. Jeong, L. Plucinski, A. DeMasi, T. Learmonth, P.-A. Glans, S. Wang, Yu. Zhang, L. F. J. Piper, P. H. Jefferson, A. Fedorov, T.-C. Chen, T. D. Moustakas, C. F. McConville, and K. E. Smith, Phys. Rev. Lett. **97**, 237601 (2006).
17. L. Colakerol, L. F. J. Piper, A. Fedorov, T. C. Chen, T. D. Moustakas, and K. E. Smith, EPL **83**, 47003 (2008).
18. A. A. Klochikhin, V. Yu. Davydov, I. Yu. Strashkova, and S. Gwo, Phys. Rev. B **76**, 235325 (2007).
19. V. Yu. Davydov, V. V. Emtsev, I. N. Goncharuk, A. N. Smirnov, V. D. Petrikov, V. V. Mamutin, V. A. Vekshin, S. V. Ivanov, M. B. Smirnov, and T. Inushima, Appl. Phys. Lett. **75**, 3297 (1999).

Translated by A. Spitsyn